Raman scattering studies in the solid electrolytes of the $RbAg_4I_5$ family

David A. Gallagher* and Miles V. Klein
Department of Physics and Materials Research Laboratory, University of Illinois at Urbana-Champaign, Urbana, Illinois 61801
(Received 21 June 1978; revised manuscript received 14 December 1978)

We have studied the dynamics of the mobile Ag^+ ions and their surrounding tetrahedral iodine cages in the solid electrolytes MAg_4I_5 (M = Rb, NH_4, K) by Raman scattering. Polarized spectra of oriented single crystals have been measured from the melting point to the second-order phase transition T_2 and to the first-order transition T_1 for KAg_4I_5. We have observed (i) a broad peak at 105 cm^{-1} of mainly A_1 symmetry which is believed to be due to the breathing modes of the crystalline cages of I^- tetrahedra, (ii) a shoulder near 20 cm^{-1} of nearly equal F_2 and E components and little A_1, which is interpreted as being due to the attempt vibrations of the silver ions, (iii) a quasielastic peak which has been assigned to the diffusive modes of the Ag^+ ions, (iv) a peak near 17 cm^{-1} having A_1 symmetry, and (v) three E peaks having frequencies near 50, 27, and X cm^{-1}, where X = 15, 17, and 18.5 for M = Rb, NH_4, and K, respectively. Except for the latter peak, the spectra are essentially identical for different M, and no new features appear below T_2.

I. INTRODUCTION

The members of the isostructural family MAg_4I_5 (M = Rb, NH_4, K) belong to a class of materials known as solid electrolytes which are characterized by their unusually high ionic conductivity. Like other solid electrolytes, MAg_4I_5 is a normal conductor at low temperature, but has a phase transition where a sublattice of a particular ionic species (Ag^+) "melts" and the ionic conductivity increases by several orders of magnitude. The resulting charged liquid of mobile ions is free to diffuse about the rigid crystalline cage composed of the nonconducting ionic species (M^+ and I^-). This paper is the last of a series of four papers concerning an investigation[1] into the dynamics of the crystalline cage and the low-frequency vibrations and diffusion of the Ag^+ ions of the MAg_4I_5 family by polarized Raman scattering. The first three publications discussed preliminary polarized Raman results for a limited temperature range of an inferior crystal of $RbAg_4I_5$,[2] Raman spectra from the internal vibrations of NH_4^+ in $NH_4Ag_4I_5$,[3] and the diffusion-related central peak region in $RbAg_4I_5$.[4] The purpose of this paper is to extend the work of the first paper to both higher and lower temperatures and to $NH_4Ag_4I_5$ and KAg_4I_5. Two previous investigations by Delaney and Ushioda[5] and Burns *et al.*,[6] were performed on nonsingle crystals. However, more complete information is obtained by performing polarized Raman measurements on single crystals.

II. STRUCTURAL ASPECTS

Each unit cell of room temperature MAg_4I_5 contains four formula units and belongs to either of the equivalent cubic space groups $P4_332$ (O^6) or $P4_132$ (O^7),[7] the latter of which is assumed in this discussion. The four Rb^+ ions are in sites of T symmetry. The 20 I^- ions are on 8 sites of C_3 symmetry and 12 sites of C_2 symmetry. Each Rb^+ ion is surrounded by 6 I^- ions on C_2 sites, the arrangement of which may be regarded as an octahedron distorted by stretching along and then twisting about one threshold axis. The 16 Ag^+ ions are distributed statistically over three nonequivalent sets of sites, totaling 56, each of which is surrounded by a distorted tetrahedron of I^- ions. The characteristics of these sets of sites are shown in Table I. Solid MAg_4I_5 has three

TABLE I. Three types of silver sites and their environments.[a]

	Ag(C_3)	Ag(C_1;II)	Ag(C_1;III)
Number of sites	8	24	24
Symmetry of sites	C_3	C_1	C_1
% of sites occupied	11	40	23
Number of Ag^+ ions per unit cell	0.9	9.5	5.5
Number of faces shared with:			
Rb^+ octahedron	1	0	0
Tetrahedra about Ag(II)	3	1	2
Tetrahedra about Ag(III)	0	2	0
Tetrahedra about Ag(C)	0	1	0
Empty tetrahedra	0	0	2

[a]Reference 7.

TABLE II. Phase-transition temperatures for MAg_4I_5.[a]

Compound	T_1 (K)	T_2 (K)	Disproportionation temperature (K)	Eutectic (K)	Incongruent melting point (K)
$RbAg_4I_5$	122	209	300	472	505
KAg_4I_5	139	194	309	512	526
$NH_4Ag_4I_5$	135	199	305	473	505

[a]Reference 8.

phases, which are labeled α, β, and γ in order of decreasing temperature. The transition temperatures between α and β and between β and γ are called T_2 and T_1, respectively, and are listed in Table II.[8] Except for a restriction forbidding nearest-neighbor occupancy of Ag sites, the Ag^+ ions are not ordered in the high-temperature phase. At T_2, there is a nearly second-order phase transition where the ionic conductivity and its derivative with respect to temperature seem to be continuous and discontinuous, respectively.[9] The crystal structure of the β phase is rhombohedral with space group $R32$ (D_3^7).[10] The skeleton lattice configuration remains essentially unchanged, but the angle between crystal axes for $RbAg_4I_5$ changes from 90° for the cubic α phase to $90.1 \pm 0.05°$ for the β phase. The distortion in the unit cell can be visualized by slightly compressing a cubic unit cell along one of the four [111] diagonals. The first-order phase transition at T_1 gives rise to a discontinuous change in the ionic conductivity of over two orders of magnitude, yet a sizable amount of disorder persists below T_1. The structure of γ-$RbAg_4I_5$, though not well understood, is trigonal and probably has the space group $P321$ (D_3^2).[10]

III. EXPERIMENTAL ASPECTS

The Raman spectra for $NH_4Ag_4I_5$ and KAg_4I_5 were excited by a Coherent Radiation model 52 argon-krypton ion laser operating at 6471 or 5682 Å at a power of about 50 mW. A Spectra-Physics helium-neon laser operating at 6328 Å at 50 mW of power excited the $RbAg_4I_5$ spectra. The polarization could be rotated 90° by a half wave plate. The beam was focused into the sample which was mounted in either a furnace[1] similar to one designed by Burns and Scott,[11] a nitrogen cryostat, or a Heli-Tran liquid-helium transfer refrigerator.

The nitrogen cryostat operated on a flow of boiling liquid nitrogen from an external Dewar. The cold gas passed through an insulated hose and a long insert in the cryostat and cooled the sample mounted at the end of the insert to as low as 100 K. Below 100 K, the Heli-Tran was used. The crystal was oriented so that the laboratory X, Y, and Z axes were along the $[1\bar{1}0]$, [110], and [001] microscopic axes of the crystal, respectively. The incident laser beam was along Z and scattered light along X was focused at 3 : 1 magnification onto the entrance slits of a Spex $\frac{3}{4}$ double monochromator, which contained Jobin-Yvon 1200-lines/mm ruled gratings, blazed at 5000 Å. In front of the slits were a polaroid and a polarization scrambler. The slits were set to give a measured resolution of 1.5 cm^{-1}. Greater stray light rejection was achieved by the use of a third monochromator consisting of a modified Perkin-Elmer Model 99 $\frac{1}{4}$-m monochromator with a Bausch and Lomb, 1200-lines/mm ruled grating, blazed at 5000 Å. The exit slit of this third monochromator was completely open and the position of the laser beam was just outside its passband. The spectral response of the third monochromator was measured and the Raman signal was corrected for the decreasing response near the laser frequency. Before every experimental run, the response was checked with a white-light source to make sure that it was exactly 20% of maximum at 3.5 cm^{-1}. Reliable Raman data could be obtained within 4 or 5 cm^{-1} of the laser frequency at 6328 Å. The combination of the Spex and a third monochromator is referred to here as a triple monochromator. The light exiting the third monochromator was detected by a cooled RCA 31034 photomultiplier tube, and the photoelectrons were counted by photon counting electronics.[12]

The Raman tensors, A_1, E, and F_2, were easily determined since the $Z(YY)X$ geometry gave $A_1 + \frac{1}{3}E + F_2$, $Z(XY)X$ gave E, and $Z(YZ)X$ or $Z(XZ)X$ gave F_2. The relative intensities of the three symmetries were obtained by separately measuring the ratios $Z(YY)X/Z(YZ)X$ and $Z(XY)X/Z(XZ)X$ at 23 cm^{-1} and making use of the relationship $Z(YZ)X = Z(XZ)X$.

IV. SAMPLE PREPARATION

MAg_4I_5 is thermodynamically unstable with respect to the disproportionation reaction $2MAg_4I_5 \rightarrow M_2AgI_3 + 7AgI$ below temperatures given in Table II. However, the rate is extremely low in a dry atmosphere. In fact, one crystal of $RbAg_4I_5$ was still optically clear after storage below 27 °C for two years. No problems associated with the disproportionation reaction were detected during the experiments reported in this work.

The disproportionation of MAg_4I_5 occurs at all temperatures in the presence of water vapor. $RbAg_4I_5$ is much more stable than the other two compounds. Exposed thin layers of $NH_4Ag_4I_5$ and KAg_5I_5 began to discolor within 5 min, while those of $RbAg_4I_5$ did not show any signs of yellowing until after a month of exposure to room air. Hence all work involving the former was done in a dry atmosphere.

The crystals were grown by evaporation of saturated HI solution[13] as follows: HI of concentration 57% was prepared by boiling reagent-grade HI of any concentration until the boiling point reached a maximum (~132 °C). About 20 g of 57% HI was heated to 50 °C and 99.9% pure AgI and then MI were added and stirred with a glass rod until dissolved. This solution was filtered through glass wool into a beaker and placed in an oven set at 1 °C above the disproportionation temperature and slowly flushed with dry air. Needles of M_2AgI_3 appeared as soon as the solution was cool, and octrahedral crystals of MAg_4I_5 appeared about one or two weeks later. At this point the solution was filtered once again, taking care that the solution did not drop below the disproportionation temperature. This saturated solution of MAg_4I_5 can be used to precipitate seed crystals or to grow large crystals from previously grown seed crystals, and the details are given by Manning *et al.*[13]

Through precession x-ray techniques, the microscopic cubic crystal axes were found to line up with the vertices of the octrahedral crystals. Thus the faces of the crystal point in {111} directions and the edges point along ⟨110⟩ directions. These facts allow one to easily orient, grind, and polish these crystals. To polish a {001} face, a special polishing block had to be designed.[1] Phenylsalicylate was used to mount the crystal to the block because it melts at about 45 °C and dissolves in trichloroethylene, one of the few solvents that does not attack MAg_4I_5. The face of the crystal was first ground and rough polished with 600 grit sand paper, and fine polishing was achieved with a Buehler microcloth, polishing pad, and 1-μ diamond paste but no oil. Finer polishing always produced a poorer surface. Al_2O_3 powder that was finer than 1 μ also did not work because it imbedded itself into the surface of the crystal.

V. EXPERIMENTAL RESULTS FOR α-MAg_4I_5

Results on α-$RbAg_4I_5$ from just below the melting point to just above the second-order phase transition are shown in Figs. 1–3. The crystal used for these results was exceptionally high in quality compared to the others and also to the crystal used for an earlier paper.[2] The rapid rise in intensity approaching the laser line from about 8 cm^{-1} is real inelastic scattering and not due to the broad Rayleigh wing, because it had been demonstrated that the elastic component is a negligible fraction of the total observed spectra if the frequency shift is greater than 5 cm^{-1}. This scattering is the subject of a separate study.[4]

The two main features in the high-temperature data are the shoulder at about 20 cm^{-1}, which is nearly equal in E and F_2 and virtually absent in A_1, and a broad peak at 105 cm^{-1} which is strongest in A_1 and much weaker in E and F_2. The ratio of the intensity of the A_1 symmetry component of the 105-cm^{-1} peak to that of the other symmetries is higher in these results than in our earlier paper.[2] The high ratio persists through the entire temperature range measured, whereas

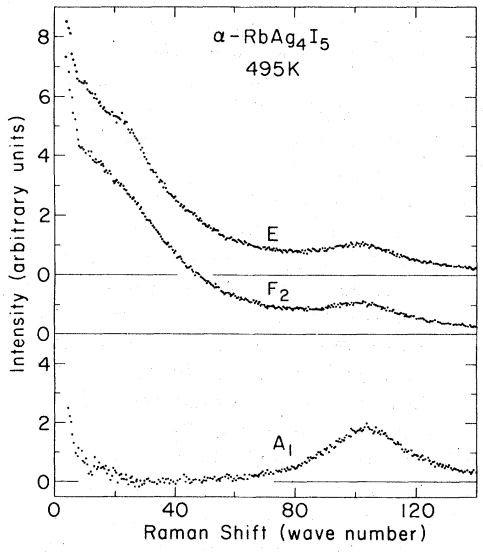

FIG. 1. Raman spectra for A_1, F_2, and E symmetries of $RbAg_4I_5$ at 495 K.

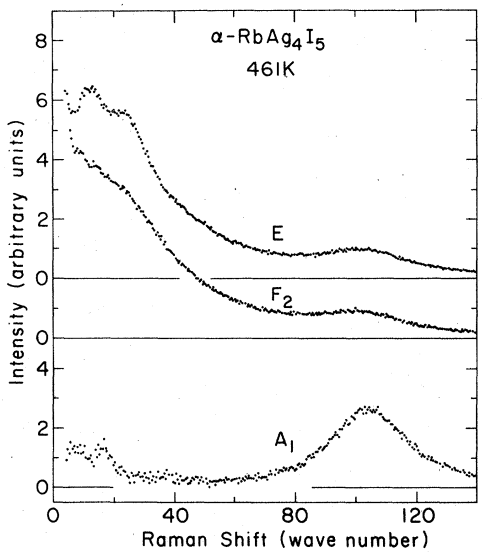

FIG. 2. Raman spectra for A_1, F_2, and E symmetries of $RbAg_4I_5$ at 461 K.

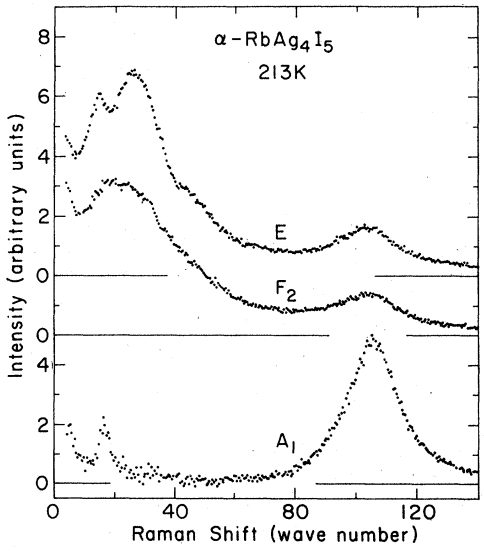

FIG. 3. Raman spectra for A_1, F_2, and E symmetries of $RbAg_4I_5$ at 213 K.

the earlier results at 210 K indicated no difference in intensity for the different symmetries. This is probably due to the surface of the earlier sample having been damaged before the spectra were measured. The 300-K results on the newer crystal, not shown here, are similar to those of Ref. 2, except that the former show about 70% more intensity of the A_1 component at 105 cm^{-1}. The appearance of these spectra differs from those of Delaney and Ushioda[5] (i.e., they observe a peak at 32 cm^{-1} instead of a shoulder at 20 cm^{-1}), because the Bose-Einstein population factor $(n+1)$ has been divided out from their data. Otherwise their data should be a weighted sum of our A_1, E, and F_2 spectra, as is the case for the results of Burns *et al.*[6]

As the temperature is lowered to 461 K, a sharp peak at 17 cm^{-1} of A_1 symmetry and two E peaks at 13 and 23 cm^{-1} appear resolved. (In the earlier work[2] these peaks were not resolved until the temperature was below 448 K.) As the temperature is lowered to room temperature, the peaks become better resolved and at 213 K, the 20-cm^{-1} shoulder in F_2 has become what seems to be a cluster of unresolved peaks. Upon cooling from 493 to 213 K, the 13- and 23-cm^{-1} peaks have hardened to 15 and 27 cm^{-1}, respectively, while the A_1 peaks at 17 and 104.5 cm^{-1} have hardened only 0 and 0.5 cm^{-1}, respectively. The full width at half maximum of the 105-cm^{-1} peak changes from 31 cm^{-1} at 493 K to 20 cm^{-1} at 213 K. At lower temperatures, a feature of E symmetry begins to appear near 50 cm^{-1}.

An intrinsic difficulty with the interpretation of polarized Raman spectra on α-MAg_4I_5 results from the fact that these crystals are optically active. The polarization direction of the incident 6471-Å polarized laser beam has been found to rotate about 5°/mm. Thus the $Z(YY)X$ and $Z(YZ)X$ geometries rotate toward $Z(XY)X$ and $Z(XZ)X$, respectively, and vice versa, assuming that the laser beam is close to the front surface of the crystal, as was the case. The F_2 spectra are not affected, but $A_1+\frac{1}{3}E+F_2$ and E mix. The amount of mixing has been calculated by integrating over the length of the image of the laser beam entering the monochromator[1] and was found to be negligible, except that the apparent intensity of the 105-cm^{-1} peak in E symmetry is about 12% larger than the true intensity. The apparent intensity, seen in Figs. 1–3, of the 105-cm^{-1} peak is about 20% higher in E symmetry than in F_2 symmetry, but the true spectra should only be about 8% different.

The temperature dependence of the Raman intensity is shown in Fig. 4. Above room temperature, the temperature dependence for $Z(XZ)X$ geometry (F_2) was measured by setting the monochromator to 23 cm^{-1} and slowly varying the temperature. At each temperature, the count rate was measured for six different laser positions within the crystal and averaged. At each position, the optics of the system were tuned for maximum Raman signal. The temperature path was retraced several times

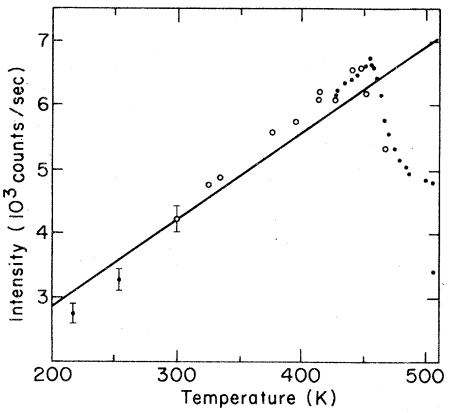

FIG. 4. Temperature dependence of the intensity at 23 cm^{-1} in F_2 symmetry. The solid line is the theoretical curve for first-order Raman scattering. Below 300 K, the plotted values were measured at 105 cm^{-1} in A_1 symmetry and converted to their equivalent values at 23 cm^{-1} in F_2 symmetry. The open circles and the dots above 420 K are discussed in the text.

to check for consistency.[1] The solid high-temperature points represent the final increase toward the melting point, and the laser position was held fixed.

The solid curve in Fig. 4 is the $n+1$ temperature dependence of first-order Stokes Raman scattering, where n is the Bose-Einstein distribution function calculated at 23 cm^{-1}. The relatively good agreement with the curve indicates that the 20-cm^{-1} shoulder is primarily first order. The large deviation from the $n+1$ curve above 180°C may be due to nonstoichiometric pockets within the crystal because the temperature at which the intensity began to drop varied among crystals from the β- to α-AgI phase transition (147 °C) to the eutectic temperature (199°). The intensity is fairly reproducible as a function of temperature below the eutectic, but not above it. Nonstoichiometric pockets contain either free AgI which transforms form β to α-AgI at 147 °C or else liquid above the eutectic.

The spectra of α-$NH_4Ag_4I_5$ and α-KAg_4I_5 are nearly identical to those of α-$RbAg_4I_5$ except the low-frequency feature in F_2 has a slightly different shape, and the low-frequency E peak has a different frequency and temperature dependence, as shown in Table III.

A problem with $NH_4Ag_4I_5$ and KAg_4I_5 crystals is that the laser beam darkens the surface upon entry and during an experimental run the Raman signal drops 1%–5%, depending on the quality of

TABLE III. Behavior of low-frequency peak of E symmetry.

	$RbAg_4I_5$ (cm^{-1})	$NH_4Ag_4I_5$ (cm^{-1})	KAg_4I_5 (cm^{-1})
Position at high temperature (just below melting)	13	16.5	17
Position at low temperature (just above T_2)	15	17	18.5
Amount of change in position	2	0.5	1.5

the crystal. (The $RbAg_4I_5$ crystal was of such high quality that no signal drop was noticed.) This was corrected by remeasuring the signal at 23 cm^{-1} immediately after every run and making a linear correction to the raw data. The darkening was found to be proportional to the total laser energy on the crystal.

The rate of darkening has an interesting temperature dependence. Within the same crystal, the rate is nearly constant above room temperature, but increases as the temperature is lowered to T_1. Below T_1, the rate of darkening (or loss of signal) decreases rapidly and is zero at 17 K. Typical values for the drop in signal during one run are a few percent above room temperature and 10%–20% at T_1. KAg_4I_5 is unusual in that, though the drop rate at room temperature is normal, the loss in signal is about 50% at T_2 and nearly 100% at T_1. The origin of this temperature dependence is not understood.

VI. SINGLE DOMAIN β-MAg_4I_5

In the β phase, MAg_4I_5 is birefringent and normally multidomained.[9] In order to perform polarized Raman scattering, the crystal must exist as a single domain. This was accomplished in $RbAg_4I_5$ by compressing the crystal between two (111) faces,[1] but no Raman data were taken. However, β-KAg_4I_5 is unique among MAg_4I_5 in that it sometimes forms spontaneously as a single domain while being cooled through the α-β phase transition.

Polarized Raman results on β-KAg_4I_5 are shown in Figs. 5 and 6 for temperatures just below T_2 and above T_1, respectively. The spectra just below T_2 are identical to the spectra just above T_2. Thus the α-β transition produces no change in the Raman spectra. Near T_1, the two low-frequency peaks of E symmetry have increased in frequency from 18.5 and 27 cm^{-1} at T_2 to 20

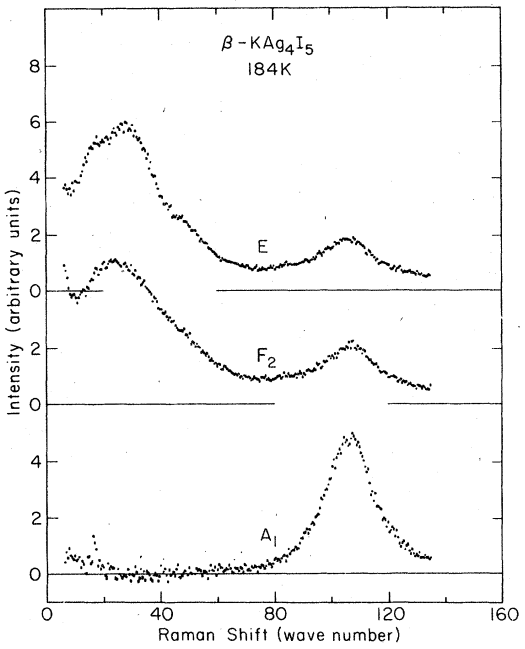

FIG. 5. Raman spectra for A_1, F_2, and E symmetries of KAg_4I_5 at 184 K.

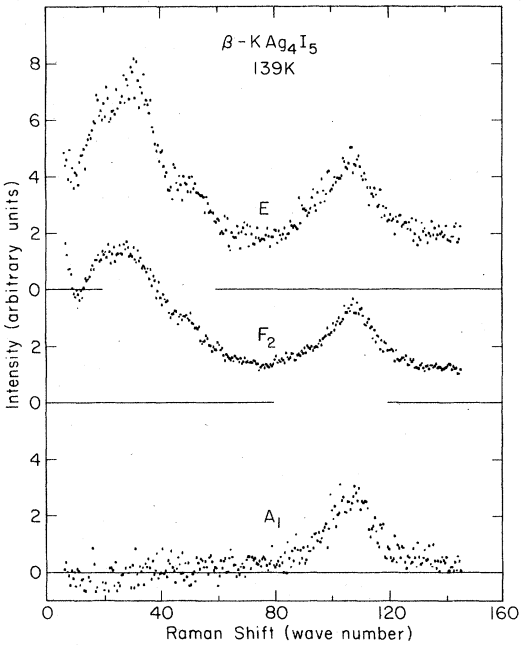

FIG. 6. Raman spectra for A_1, F_2, and E symmetries of KAg_4I_5 at 139 K.

and 31 cm^{-1}, respectively, at T_1. At T_1, the data are very noisy because the rate of darkening of the crystal is extremely large at that temperature, and the spectra had to be taken very quickly in order to reduce the time of exposure of the crystal to the laser beam.

VII. MULTIDOMAINED β- AND α-MAg_4I_5

As mentioned in the previous section, polarized Raman scattering usually cannot be performed below T_2, so unpolarized spectra were measured. (A double monochromator was used alone for these spectra, and the low-frequency rise in intensity near the laser line is partially due to elastic laser scattering.)

Figure 7 shows unpolarized spectra for $RbAg_4I_5$. Since there is no change in the spectra through T_2, the spectrum at 208 K is essentially a weighted sum of the three spectra in Fig. 3, which was taken slightly above T_2. The temperature dependence in β-$RbAg_4I_5$ is quite evident from Fig. 7. As the temperature is lowered from above the β-γ transition to 17 K, the spectra are characterized by (i) a sudden and reproducible appearance of a 22-cm^{-1} peak at the transition temperature, (ii) a gradual splitting and resplitting of the above T_1 features as the temperature is lowered below T_1, and (iii) the continued presence of the 17-cm^{-1} peak. The second of the above facts supports Geller's statement that at 90 K, the phase is still disordered.[10] The ordering seems to increase with decreasing temperature.

There is little difference among the spectra of γ-MAg_4I_5 for different M. The difference amounts to only a slight shift in frequency for corresponding peaks and different relative amplitudes. Table IV summarizes all the data for γ-MAg_4I_5. From this table, one can see which peak in KAg_4I_5 and $NH_4Ag_4I_5$ corresponds to each peak in $RbAg_4I_5$.

For the most part, the unpolarized spectra were quite reproducible, except for α-KAg_4I_5 near 100 K, where relative sizes of the peaks changed drastically from one run to another during a set of multiple runs on the same crystal. No correlations were found between the appearance of the spectra and either (i) scattering geometry, (ii) age of the crystal, or (iii) laser exposure time.

VII. DISCUSSION

To interpret the Raman spectra for α-MAg_4I_5, the usual application of group theory is not valid for MAg_4I_5 because the configuration of Ag^+ ions in any given unit cell is not repeated in neighboring cells. We therefore propose a "random tetrahedral" model based on the following con-

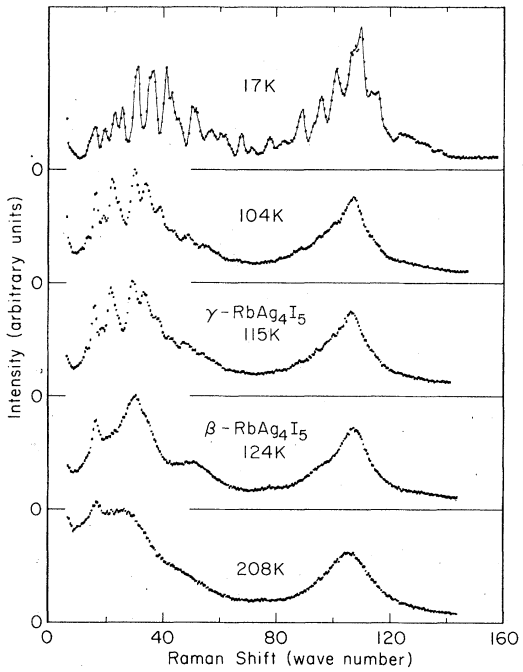

FIG. 7. Unpolarized Raman spectra of $RbAg_4I_5$ at 208, 124, 115, 104, and 17 K.

siderations. The Ag^+ sites are surrounded by distorted tetrahedra of I^- ions. Because of the great amount of disorder, each Ag^+ ion and its four nearest I^- neighbors can be treated as an AgI_4^{3-} ion which has the vibrational properties of an XY_4 molecule of T_d symmetry. The 56 I^- tetrahedra are oriented in so many different directions that the distribution of orientations is nearly random. Thus the AgI_4^{3-} "molecules" form a nearly isotropic "liquid" within the crystal. In an isotropic liquid, all off-diagonal terms in the polarizability tensor are equal. Therefore, in the crystal the Raman contribution from an E mode or F_2 mode in AgI_4^{3-} will have equal E and F_2 intensities in the crystal. The A_1 mode in AgI_4^{3-} will only contribute to the A_1 Raman intensity in the crystal.

The Ag^+ ions vibrate very slowly and anharmonically in their respective tetrahedral I^- cages. For AgI_4^{3-}, these Ag^+ displacements would belong to T_d modes of type ν_3. Thus the crystal's Raman contribution from the Ag^+ ions should be equal in F_2 and E and zero in A_1 symmetry, which is consistent with the observed shoulder at 20 cm^{-1} in the spectra at high temperature and its polarization properties. This Raman peak agrees with the results of the dynamic structure factor from neutron scattering, which gives evidence of overdamped vibrations in the vicinity of 20 cm^{-1}.[14]

In the high-frequency end of the spectra, we find a broad peak at 105 cm^{-1} which is strongest in A_1 symmetry. Similar features are found in other solid electrolytes where each mobile cation is surrounded by a tetrahedron of I^- ions. In the high-temperature phase of AgI,[15] there is a broad shoulder near 90 cm^{-1} which is much stronger in the A_1-rich polarized Raman spectra than in the depolarized spectra. Also, in the solid electrolyte phase of Ag_2HgI_4,[16,17] where both the Ag^+ ions and the Hg^+ ions are mobile, Greig *et al.* have assigned a large peak at 124 cm^{-1} to the symmetric HgI_4^{2-} stretching mode. They have also assigned the peak at 45 cm^{-1} to silver-iodine stretching modes, but the symmetry of the peak is unknown. Thus in all three materials there is a feature near 100 cm^{-1} which seems to result mostly from symmetric (A_1-like) vibrational modes. We therefore propose that this higher-frequency feature is primarily due to the A_1 (or ν_1) breathing modes of the tetrahedral iodine cages. It might be noted that the broad 105-cm^{-1} peak is of equal intensity in E and F_2 symmetry. This is consistent with the possibility that the 105-cm^{-1} peak of E and F_2 symmetry results from the combination of the E and T_d (ν_4) bending modes of the AgI_4^{3-} "molecule."

Even though it is not possible to apply group theory to the MAg_4I_5 structure as a whole, it might be profitable to apply the theory to only the rigid crystalline frame of M^+ and I^- ions which we refer to as MI_5 (MAg_4I_5 without the Ag_4). Applying the correlation method of group theory to MI_5, one obtains the following representations for the normal modes of MI_5:

$$\Gamma_{MI_5} = 2A_1 + 4A_2 + 6E + 10F_1 + 8F_2 . \tag{1}$$

The representations for the Raman-active modes involving the motion of the 4 M^+ ions, the 12 I^- ions on sites of C_2 symmetry, and the 8 I^- ions on sites of C_3 symmetry are

$$\Gamma'(M) = E + F_2 , \tag{2}$$

(motion perpendicular to [111] axis)

$$\Gamma'(\mathrm{I}; C_2) = A_1 + 3E + 4F_2 , \tag{3}$$

$$\Gamma'(\mathrm{I}; C_3) = A_1 + 2E + F_2 , \tag{4}$$

where

$$\Gamma_{MI_5} = \Gamma'(M) + \Gamma'(\mathrm{I}; C_2) + \Gamma'(\mathrm{I}; C_3) + \cdots ,$$

where the dots represent non-Raman-active terms.

Hence, the vibrations of the I^- ions are described by two different modes: (i) as part of AgI_4^{3-} ions, and (ii) as part of a perfect MI_5 lattice. Since the disorder washes out most of

TABLE IV. Comparison of peak and shoulder positions for different M and temperatures. Shoulders are indicated by (sh).

	$RbAg_4I_5$				$NH_4Ag_4I_5$				KAg_4I_5		
124 K	115 K	104 K	17 K	137 K	134 K	104 K	17 K	142 K	136 K	103 K	17 K
										(sh)10	(sh)9.5
		(sh)14	(sh)14.5	17	(sh)15	(sh)15	(sh)16		15	15.5	16.5
17 cm^{-1}	16.5	17	16.5		17.5	17.5	18	(sh)17	17	17	(sh)18
	19	19.5	20								
	22	22.5	23.5		23	22.5	24	23	22.5	22.5	23.5
		(sh)25	26			26	28		29.5	29.5	29
31	30	30.5	31	31	31	31.5	34	30.5		(sh)31.5	32
(sh)34	34	34.5	37		36	37	37.5		36.5	37	37
	(sh)38	39.5	41				40.5			40	39
			43			(sh)41	42				42.5
	(sh)43	(sh)44.5	(sh)46				47		(sh)45	(sh)46	45.5
											48
	48	49	51			(sh)49	51		51	52	54
			52				(sh)53				
(sh)52	(sh)56	57	57	(sh)53			57	(sh)53	(sh)57.5	(sh)59	
			60.5			60	61.5				62.5
			62.5				63.5				65
			68				66.5				70
			71.5				72.5			72	72
			78				77				76
											78.5
			83				81				81
	(sh)88	(sh)89	89				89.5				86.5
			(sh)93								92
(sh)94	(sh)94.5	(sh)95	95.5				96		(sh)92	94	95
											(sh)99
	(sh)100	(sh)101	101				102.5		(sh)102	102.5	103
107	107	107	(sh)107	107	107	107.5	108	108	108		(sh)108
			110				110.5			110	110
			113.5				116				113
			115.5								114.5
			124				124				125
			132				127				131
			138				136				135
							148				143

the fine structure that would appear in the spectra if there really were a perfect MI_5 lattice, the AgI_4^{3-} random tetrahedral model is nearly correct, except for features resulting from remnants of the MI_5 periodicity which might be the peaks at 17 cm^{-1} in A_1 symmetry and 15, 27, and 50 cm^{-1} in E symmetry, which are not explained by the random tetrahedral model. It is interesting to speculate that the 17-cm^{-1} peak is the A_1 mode involving the I ions at C_2 sites. This is a symmetric twisting mode of the octrahedra around the M^+ ions. The I^- ions move nearly tangentially toward the M^+ ions, while the two equilateral triangles of I^- ions at each end along the [111] axis of the octahedron expand and rotate slightly. This mode has much less bond stretching (and therefore a lower frequency) than the A_1 mode from the I(C_3) ions which involves four pairs of breathing I^- ions with their axes along the four [111] axes. This other mode could be part of the AgI_4^{3-} breathing modes discussed above. Actually, the 17- and 105-cm^{-1} peaks would probably be linear combinations of the two A_1 modes from I(C_3) and I(C_2) ions. The 15-, 27-, and 50-cm^{-1} peaks could be three or more of the five E modes of the I ions. The 15-cm^{-1} peak could involve the M^+ ions as well, since this peak is M-dependent and the representation for the M^+ ions contains one mode of E symmetry.

A major difficulty with making commitments to the interpretations of the previous paragraph is that vibrations of the Ag^+ ions are expected to have low frequencies on the order of 20 cm^{-1}, whereas the M^+ and I^- ions should oscillate closer to 100 cm^{-1}. There are other possible vibrational modes involving the Ag^+ ions such as: (i) two Ag^+ ions vibrating against each other, (ii) an $Ag^+(C_3)$ or $Ag^+(C_1;\mathrm{III})$ ion vibrating against its neighboring M^+ ions, and (iii) many others involving multiple Ag^+ ions. However, it is hard to believe that overdamped vibtations involving Ag^+ ions would result in such narrow peaks. The vibrations of pairs of Ag^+ ions would be oriented in so many different directions that E and F_2 should be equal.

IX. CONCLUSION

We have studied and have gained insight into the dynamics of the crystalline cage MI_5 and the charged liquid of the mobile Ag^+ ions in MAg_4I_5 (M = Rb, NH_4, K). Above T_1, the temperature at which MAg_4I_5 becomes a solid electrolyte, there are three major features. These are: (i) a broad structureless peak at about 105 cm^{-1} which is much stronger in A_1 symmetry, (ii) a broad feature near 20 cm^{-1} which has roughly equal F_2 and E components and little A_1 intensity, and (iii) quasielastic peaks centered about the laser line which are interpreted as due to the diffusive motion of the Ag^+ ions.[4] The first two features are explained by assuming that all Ag^+ ions and their tetrahedral cages of nearest-neighbor I^- ions are equivalent to a liquid of AgI_4^{-3} ions. The 105-cm^{-1} peak is thought to be due primarily to the symmetric breathing mode of the AgI_4^{3-} ion and the 20-cm^{-1} feature is interpreted as the attempt vibrations of the Ag^+ ions. At high temperature, the 20-cm^{-1} feature appears as a quasielastic peak, but at lower temperatures, the feature looks more like a cluster of peaks centered about 20 cm^{-1}. This indicates that the Ag^+ vibrations are overdamped at high temperature.

At lower temperature, but above T_1, the above mentioned broad features have sharper peaks superimposed over them. These peaks can be accounted for only in a speculative way by assuming that they result from the lattice vibrations of the rigid crystalline cage.

There are no changes in the spectra at the second-order phase transition at T_2, except that for $M \neq$K, the polarization becomes mixed and, hence only unpolarized spectra can be taken. Below T_1, no abrupt changes occur, except a sharp new peak appears at 22 cm^{-1}. As the temperature is lowered, the regular features, except for the 17-cm^{-1} peak, split and sometimes split again. Finally at 17 K, there are about 25 fairly sharp peaks, the envelope of which resembles the smooth features above T_1. The peaks are the same for different M, except for slight differences in frequencies and relative intensities. The 17-cm^{-1} peak is present in all three phases of MAg_4I_5 and changes by less than 1 cm^{-1} through the entire temperature range.

ACKNOWLEDGMENTS

We thank F. L. Lederman and R. A. Vargas for their help in growing the crystals. This work was supported in part by the NSF under the MRL Grants No. DMR-76-01058 and DMR-77-23999.

*Present address: Defense Systems Division, Northrop Corp., 175 W. Oakton St., Des Plaines, Ill. 60018.

[1] D. A. Gallagher, Ph.D. dissertation (University of Illinois, Urbana, 1978) (unpublished).
[2] D. Gallagher and M. V. Klein, J. Phys. C 9, L687

(1976).
[3]D. A. Gallagher and M. V. Klein, J. Chem. Phys. 68, 4804 (1978).
[4]R. Field, D. Gallagher, and M. V. Klein, Phys. Rev. B 18, 2995 (1978).
[5]M. J. Delaney and S. Ushioda, Solid State Commun. 19, 297 (1976).
[6]G. Burns, F. H. Dacol, and M. W. Shafer, Solid State Commun. 19, 287 (1976).
[7]S. Geller, Science 157, 310 (1967).
[8]B. B. Owens, *Advances in Electrochemistry and Electrochemical Engineering*, edited by C. W. Tobias (Wiley, New York, 1971), Vol. 8.
[9]F. L. Lederman, M. B. Salamon, and H. Peisl, Solid State Commun. 19, 147 (1976).
[10]S. Geller, Phys. Rev. B 14, 4345 (1976).
[11]G. Burns and B. A. Scott, Phys. Rev. B 7, 3088 (1973).
[12]J. A. Holy, Ph.D. dissertation (University of Illinois, Urbana, 1977) (unpublished).
[13]M. R. Manning, C. J. Venuto, and D. P. Boden, J. Electrochem. Soc. 118, 2031 (1971).
[14]S. M. Shapiro, D. Semmingsen, and M. Salamon, *Proceedings of the Semiconductor Conference*, edited by M. Balkanski (Flammarion Sciences, Paris, 1977).
[15]R. C. Hanson, T. A. Fjeldly, and H. D. Hochheimer, Phys. Status Solidi B 70, 567 (1975).
[16]J. Hiraishi and W. G. Fateley (unpublished).
[17]D. Greig, D. F. Shriver, and J. R. Ferraro, J. Chem. Phys. 66, 5248 (1977).